

Bound state and hydrodynamic interaction of microrods in chiral nematic liquid crystals

Muhammed Rasi M¹, Ravi Kumar Pujala², Sathyanarayana Paladugu², and Surajit Dhara^{1*}

¹*School of Physics, University of Hyderabad, Hyderabad-500046, India*

²*Department of Physics, Indian Institute of Science Education and Research, Tirupati, Andhra Pradesh 517507, India*

(Dated: February 28, 2025)

In a striking departure from the pair interaction of spherical microparticles in chiral nematic liquid crystals we show that a pair of microrods form a bound state due to the competing effect of electrostatic and elastic interactions. The robustness of the bound state is demonstrated by applying external electrical and mechanical forces that perturbs their equilibrium position as well as orientation. In the bound state the microrods interact through the hydrodynamic forces which are determined from the measurements of the correlated thermal fluctuations in their position using two-particle cross-correlation spectroscopy. These findings reveal unexplored aspects of liquid-crystal dispersions which are important for understanding the assembly and dynamics of the nano and microparticles in chiral nematic liquid crystals.

Microparticles in nematic liquid crystals (NLCs) create spatial deformation of the director \hat{n} (mean molecular orientation), and induce topological point or line defects [1–3]. The defect structures and the ensuing elastic distortion mediated long-range interactions have created immense interests in recent years owing to the potential application for designing two and three dimensional colloidal crystals [4, 5]. When the dispersing medium is a chiral nematic the director twists in space, exhibiting a number of interesting defects that includes vortex-like nonsingular defects [6, 7], knots and links [8], torons [9], skyrmions [10, 11] etc. These defects and the resulting elastic interaction of spherical microparticles often leads to metastable [12] and reconfigurable states [8, 13, 14].

Apart from elastic interaction, electrostatic and hydrodynamic interactions of microparticles in liquid crystals play an important role in their assembly and structure. Recently some interesting aspects of electrostatic interaction of particles in nematic LCs has been experimentally demonstrated [15–17]. Theoretically hydrodynamic effects in LC colloids has been studied [18–20] but not directly explored experimentally. The hydrodynamic interaction has been studied directly in aqueous colloidal systems by optically trapping two Brownian particles using laser tweezers [21, 22]. However, the particles in LCs can not be directly trapped by laser tweezers in the conventional way [23, 24] thus making the direct measurement of hydrodynamic interaction problematic in LCs.

In this letter we report experimental studies on individual silica microrods in chiral NLCs and show that the competing effect of electrostatic and elastic pair interaction leads to a bound state, in which they are separated by a fixed distance. We show that the trapping is robust against external perturbations that tends to change their position as well as orientation. Our experiments present a direct measurement of the hydrodynamic interaction of microparticles revealing an unexplored aspect of liquid crystal dispersions.

Silica microrods are synthesised by a wet chemical method following a procedure described by Kuijk *et al.* [25, 26]. The average length and diameter are 6 μm and 800 nm, respectively and one end of the microrods is round-shaped as shown in Fig.1(a). The microrods were coated with octadecyldimethyl-3-trimethoxysilyl propyl-ammonium chloride (DMOAP) before dispersing into the chiral NLCs for obtaining perpendicular or homeotropic orientation of the director \hat{n} . The chiral NLCs were prepared by doping a chiral agent 4-cyano-40-(2-methylbutyl)-biphenylene (CB15) in 4-n-pentyl-4-cyanobiphenyl (5CB) nematic liquid crystal. The concentration of CB15 was adjusted to vary the helical pitch, which was measured using a wedge cell [27]. The dispersions were studied in planar cells, which are prepared by two parallel glass plates (15 mm \times 10 mm) coated with the polyimide AL-1254 (Nissan Chemicals). The plates were rubbed in an antiparallel way before assembling so that the helix axis of the chiral NLC is perpendicular to the plane of the substrate as shown in Fig.1(b). The pitch was adjusted in a cell of gap d such that the nematic structure is twisted by multiples of half-pitch i.e., $d = N(p/2)$ which is denoted here as $N\pi$ cell (Fig.1(b)). An infrared laser tweezers setup (Aresis, Tweez 250Si) attached to an inverted optical polarising microscope (Nikon Eclipse Ti-U) was used in the experiments [28–30]. The laser trap movement was controlled by an acousto-optic deflector (AOD) and computer. The motion of the microrods were video recorded using a 60X water immersion objective (Nikon NIR Apo) and a camera at the rate of 50 frames per second. The centre of the microrod was measured from the video-microscopy with a resolution of ± 20 nm [31, 32]. The autocorrelation and cross-correlation functions of the position fluctuations were computed using the Mathematica program.

We work in the dilute concentration regime where most of the microrods are dispersed singly throughout the cell. At first, we study the LC-microrod dispersions in a 2π cell and observe that the majority of the microrods are orientated perpendicular to the rubbing direction (Fig.1(c)). Although the surrounding elastic distortion of the micro-

* sdsp@uohyd.ernet.in

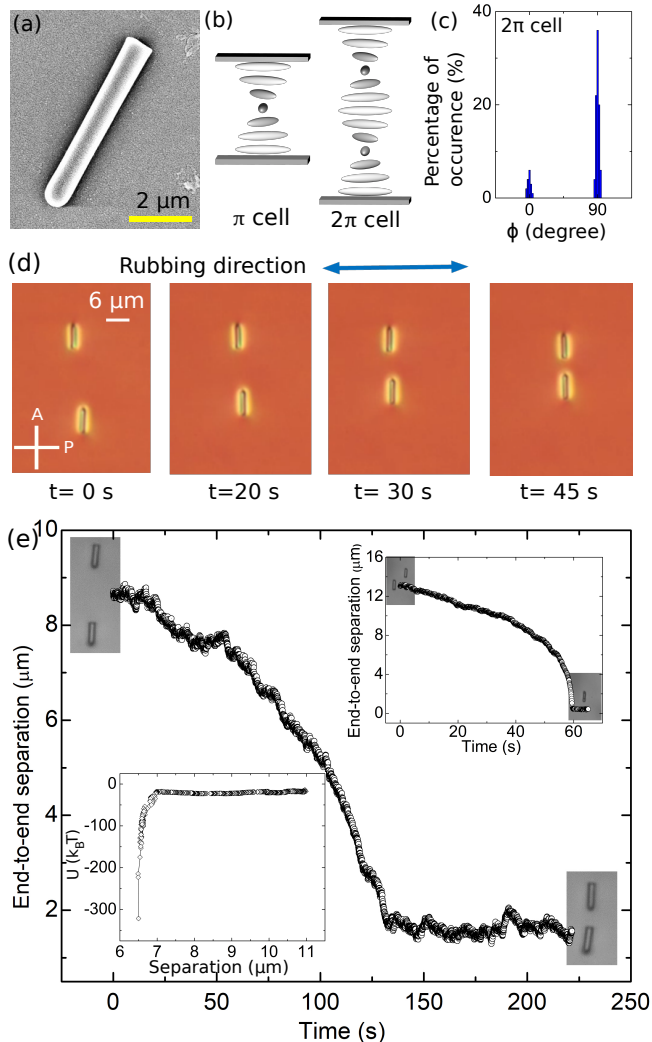


FIG. 1. (a) Field emission scanning electron microscope (FESEM) image of a silica microrod. (b) Director twist in π and 2π cell. (c) Percentage of microrods oriented parallel ($\phi \simeq 0^\circ$) and perpendicular ($\phi \simeq 90^\circ$) with respect to the rubbing direction in 2π cell. (d) Snapshots of interacting microrods at different times taken using polarising optical microscope. Horizontal arrow indicates the rubbing direction. P, A indicates polariser and analyser. (e) End-to-end separation of two interacting microrods in 2π cell (Movie S1). The upper inset (right corner) shows the end-to-end separation in a planar, homogeneous nematic (5CB). The bottom inset (left corner) shows the elastic interaction potentials while approaching to form bound state in 2π cell.

rod is clearly visible, the structure of the defect is unclear unlike the case of a microsphere (Fig.1(d)). We study the pair interaction of microrods orientated perpendicular to the rubbing direction in a 2π cell. Two coaxial microrods were positioned at a certain distance away with the help of the laser tweezers and allowed them to interact freely by switching off the laser. Figure 1(d) shows a few snapshots at different times while they are approaching

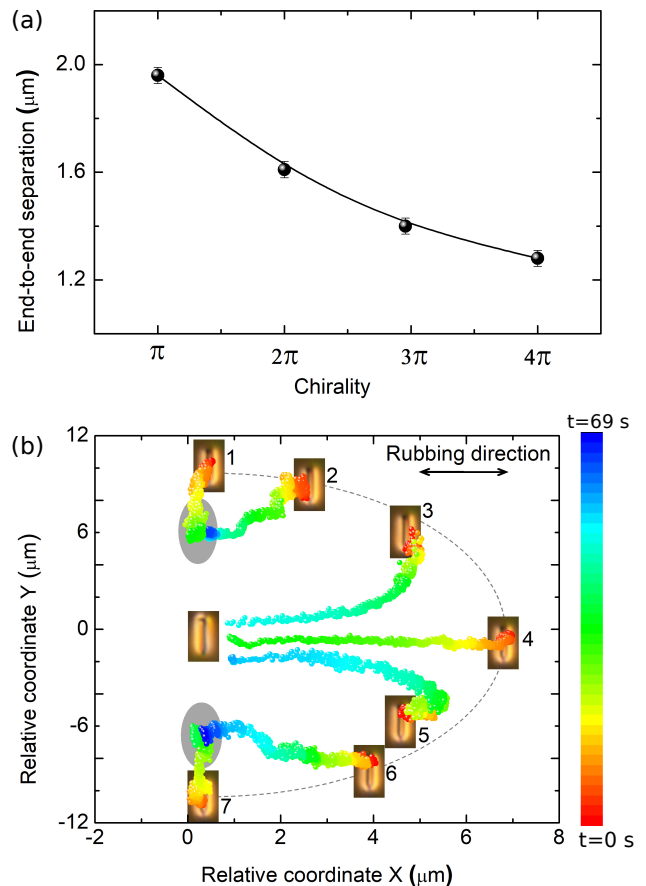


FIG. 2. (a) Variation of end-to-end separation with chirality in the bound state. (b) Time coded trajectories (relative coordinates) of microrods approaching from different starting positions in 2π cell. By “relative coordinate” we mean relative to the starting point of each trajectory. Shaded regions indicate where the approaching particle is permanently bound with the central particle.

to each other. With increasing time the end-to-end separation decreases and eventually the microrods are self-confined or trapped at a fixed separation forming a bound state as shown in Fig.1(e). The mean separation between the microrods in the bound state (beyond 130 s) is $1.65 \mu\text{m}$ and it remains fixed forever (see Fig.S1). It appears as if the microrods are trapped in the global energy minimum. Similar behaviour is also observed in cells with different chiralities except the end-to-end separation decreases moderately with increasing chirality as shown in Fig.2(a). The interaction in chiral NLCs is noticeably different than that is observed in a planar or homogeneous nematic where the end-to-end separation is reduced to zero as shown in the inset of Fig.1(e). Spherical microparticles in chiral NLCs exhibit metastable states due to the screening of chiral interaction in which the microspheres are temporarily held at a fixed separation for a certain period of time and eventually they are attracted and joined together [12]. The striking result of our experiment is

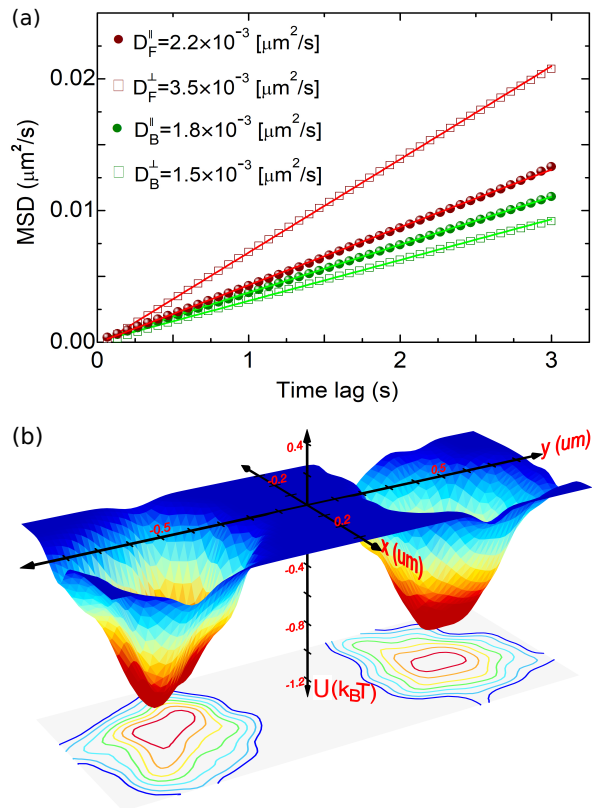


FIG. 3. (a) Mean squared displacements (MSDs) of a free microrod (red symbols) and a bound microrod (green symbols) in 2π cell. The subscripts F and B stands for free and bound microrods, respectively and the superscripts \parallel and \perp indicate motions parallel and perpendicular to the rubbing direction. (b) Confining potentials of the bound microrods. Separation along the y -direction is normalised.

that the microrods are permanently self-trapped forming a stable bound state without merging. The origin of the bound state can be understood based on the competing effect of the electrostatic and elastic interactions. Usually the surface of the silica microrods are highly charged [33]. We measured the zeta potential of the microrods dispersed in ethanol using an electrophoretic light scattering technique and found $\Psi_0 = -13 \pm 1$ mV. To see the effect of surface charge we heated the sample to the isotropic phase where the elastic interaction of the liquid crystal is absent and pushed the microrods towards each other with the help of laser tweezers (see Movie S2). The microrods stay away from each other against the impelling force demonstrating an electrostatic repulsion between them due to the surface charge. The surface charge density is given by $\delta = \epsilon_0 \epsilon \Psi_0 / \lambda_D$ [34], where λ_D is the Debye screening length. Assuming $\lambda_D \approx 100$ nm [16, 35], and $\epsilon \approx 10$, the calculated surface charge density is given by $\delta \approx 1.2 \times 10^{-5}$ As/m². This gives rise to an approximate total charge of a microrod $Q = 1600e$ and an electrostatic repulsion energy of 17.5×10^3 K_BT. Thus repulsive electrostatic potential energy is more than one order of

magnitude larger than the attractive elastic energy (300 K_BT) of the microrods (see inset Fig.1(e)). Hence, the metastable state becomes bound state due to the electrostatic repulsion between the microrods.

The anisotropy of the pair interaction was studied by looking at the relative time coded trajectories of microrods released from different starting positions with respect to a central microrod as shown in Fig.2(b). Microrods starting from the positions 1,2,6 and 7 are attracted to form the bound state whereas the microrods released from the starting positions 3,4,5, are merge eventually. The elastic attractive interactions in latter positions are stronger compared to the electrostatic repulsion between the microrods.

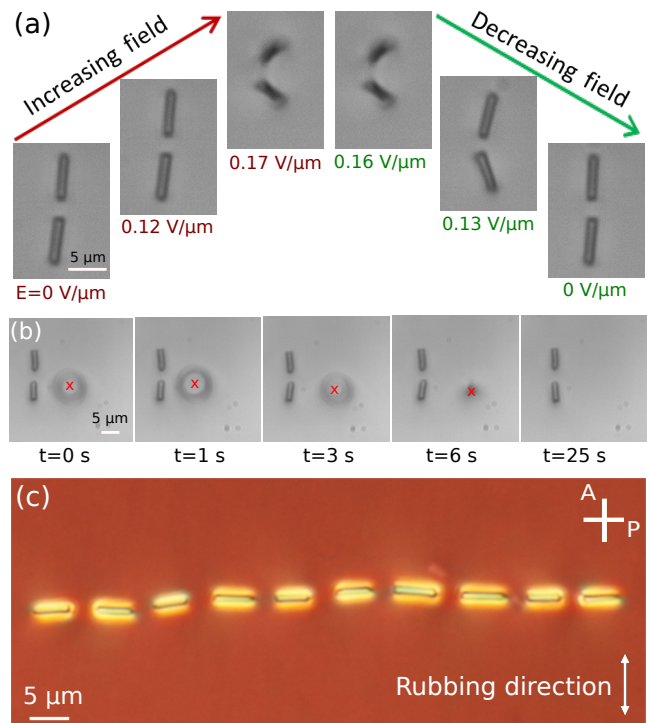


FIG. 4. (a) Effect of AC electric field ($f = 1$ kHz) on the bound state in 2π cell (Movie S3) (b) Effect of mechanical force applied by the laser tweezers on the bound state. (Movie S4) (c) A linear chain of 10 microrods forming successive bound states (Movie S5). They were guided to assemble with the help of a dynamic laser tweezers setup.

In the bound state the Brownian motions due to thermal agitations of the microrods are clearly observed (see Movie S1). The self-diffusion coefficients $D_B^{\parallel, \perp}$ of a bound microrod and $D_F^{\parallel, \perp}$ of a free or isolated microrod (where \parallel and \perp refers in relation to the rubbing direction) were obtained from the mean squared displacement. Figure 3(b) shows that $D_B^{\perp} \approx 0.4 D_F^{\perp}$ and $D_B^{\parallel} \approx 0.8 D_F^{\parallel}$ i.e., the diffusion coefficients in the bound state are reduced considerably than that of a free microrod as expected. We measured the effective confining potentials from the study of the Brownian statistics of the microrods in the region

accessible by thermal agitations [36]. In equilibrium the probability density of the particle position is given by $p(x) = C \exp[-U(x)/k_B T]$, where C is the normalisation constant and $U(x)$ is the confining potential. The potential is obtained from the normalised histogram of the confined particle's positions and given by $U(x) = -\ln[p(x)]$. Figure 3(b) shows the confining potentials of the microrods at a normalised centre-to-centre distance. The depth of the potential energy is $\sim k_B T$ and highly asymmetric as expected (see contour plots). Assuming the potentials are harmonic, the effective stiffness constants k_x (along rubbing direction) and k_y (perpendicular to the rubbing direction) are given by $k_x = 4.3 \pm 0.1 \times 10^{-6}$ N/m and $k_y = 4.8 \pm 0.1 \times 10^{-6}$ N/m. The stiffness constants of the confining potentials are comparable to that of the low power optical traps [21, 38].

To test the robustness of the bound state we applied an external AC electric field that perturbs the position and orientation of the microrods (Movie S2). Fig.4(a) shows some snapshots at different field strengths. The maximum field was restricted to the Freederickzs threshold value ($\simeq 0.2$ V/ μm) so that the far field director remains unaffected. Beyond $\simeq 0.12$ V/ μm , the microrods are displaced (see Fig.S2) and they also tilt simultaneously in the plane as well as out of the plane. The initial state is recovered when the electric field is switched off. We further checked the stability by applying a mild mechanical force with the help of the laser tweezers as shown in Fig.4(b). It is observed that the bound state is stable against the elastic distortion created by the trap surrounding the microrods (Movie S3). With the help of the laser tweezers we have created an assembly of several microrods in the form of a linear chain as shown in Fig.4(c). Here the microrods are virtually linked through the successive bound states. The chain is little zigzag which could be due to the slight variation in the length and diameter of the microrods. Nevertheless the chain is stable against thermal fluctuations and mild perturbing force applied by the laser tweezers (Movie S6) and remains unchanged even after a few days. It may be mentioned that although one end of the microrods is round-shaped the bound state formation does not depend on the shape of the facing ends.

In what follows we study the hydrodynamic interaction of the microrods in the bound state. Hydrodynamic interaction of particles in aqueous solution has been studied by optically trapping a pair of microspheres at varying proximity [21, 22]. In our experiment the bound state of the microrods is a reminiscent of similar experimental situation, providing an opportunity to measure directly the hydrodynamic interaction. We measure the position and calculate the autocorrelation and cross-correlation functions. In the framework of Langevin dynamics for a low Reynolds number system the autocorrelation and the cross-correlation functions of position vectors of the two particles along y-direction (perpendicular to the rubbing direction) are given by [21]

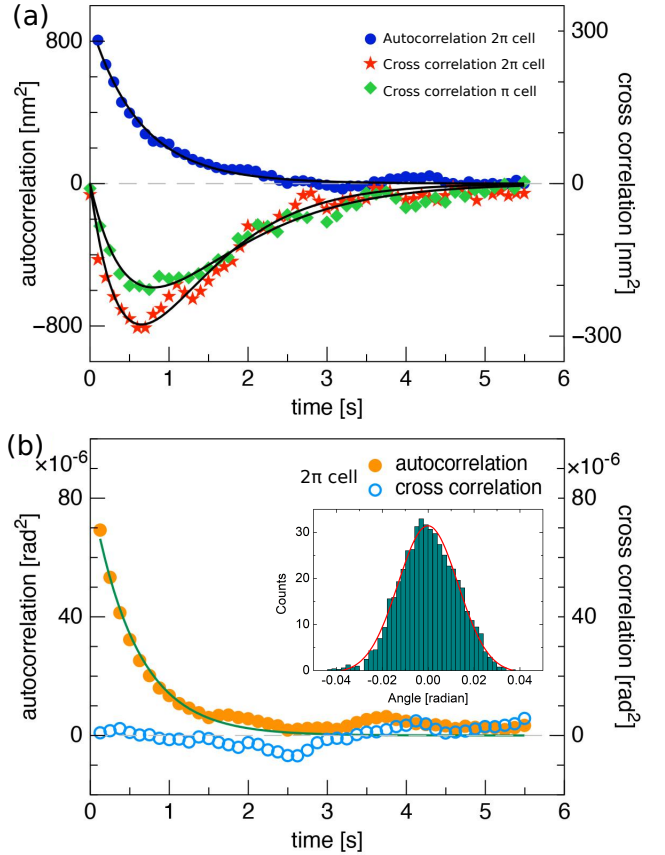


FIG. 5. (a) Longitudinal autocorrelation $\langle R_1(t)R_1(0) \rangle$ (blue circles) and cross-correlation $\langle R_1(t)R_2(0) \rangle$ (green diamonds and red stars) functions of the two microrods in π and 2π cells. Solid lines represent the best fit to Eq.(1). (b) Autocorrelation function $\langle \theta_1(t)\theta_1(0) \rangle$ (solid circles) and cross-correlation function $\langle \theta_1(t)\theta_2(0) \rangle$ of orientational fluctuations (open circles) of two microrods in 2π cell. θ_1 and θ_2 are measured with respect to the vertical axis (see Fig.1(d)). Only every third of the experimental data points is shown. The inset shows the histogram of a orientational deviation.

$$\begin{aligned} \langle R_1(t)R_1(0) \rangle &= \langle R_2(t)R_2(0) \rangle \\ &= \frac{k_B T}{2k_y} (e^{-t(1+\epsilon)/\tau} + e^{-t(1-\epsilon)/\tau}) \end{aligned} \quad (1)$$

$$\begin{aligned} \langle R_1(t)R_2(0) \rangle &= \langle R_2(t)R_1(0) \rangle \\ &= \frac{k_B T}{2k_y} (e^{-t(1+\epsilon)/\tau} - e^{-t(1-\epsilon)/\tau}) \end{aligned} \quad (2)$$

where τ is the relaxation time and ϵ is a dimensionless parameter. The autocorrelation and cross-correlation functions measured in π and 2π cells and the theoretical fits to Eq.(1) and Eq.(2) are shown in Fig.5(a). The parameters obtained from the fittings are given by $\tau = 0.64 \pm 0.01$ s and $\epsilon = 0.10 \pm 0.01$. The autocorrelation function decay

exponentially as expected whereas a strong time delayed-anticorrelation is observed with a pronounced minimum at $t_{min} \approx \tau \simeq 0.64$ s. It means the hydrodynamic interaction is asymmetric as one microrod moves it tends to drag the other and the correlated fluctuations relax faster than the anticorrelated fluctuations. We directly measure ϵ from the particle separation and τ from the effective confining potentials. τ is given by the ratio of the friction coefficient ζ_y and the stiffness constant k_y of the potential i.e., $\tau = \zeta_y/k_y$. The parameter ϵ describes the ratio of the mobility of the particle and the strength of the hydrodynamic coupling and expressed as $\epsilon \approx 3a/2r$, where r is the mean separation and a is the radius of the particle [21]. From the measured diffusion coefficient (Fig.3(a)) we obtain $\zeta_y = 2.8 \times 10^{-6}$ Kg/s using Stokes-Einstein relation and $k_y = 4.8 \times 10^{-6}$ N/m from the confining potentials (Fig.3(b)). Taking radius of the microrod $a = 0.4 \mu\text{m}$ and centre-to-centre separation $r \simeq 7 \mu\text{m}$ the measured parameters are $\tau = 0.58$ s and $\epsilon \simeq 0.09$. These parameters are in good agreement with those obtained from the fitting of the autocorrelation and cross-correlation functions. It is also observed from Fig.5(a) that the depth of the minima in 2π cell is higher than that of π cell. In 2π cell the particles are closer than π cell (Fig.2(a)) hence, the result is consistent with the prediction that the strength of the hydrodynamic coupling is inversely proportional to the separation [21].

In the bound state the orientational fluctuations of the microrods are clearly observed. The orientational fluctuations θ_1 and θ_2 of the long axis of the microrods is measured with respect to a vertical axis (see Fig.1(d)). The histogram of the orientational fluctuations is a Gaussian as shown in the inset of Fig.5(b). We measure the autocorrelation $\langle \theta_1(t)\theta_1(0) \rangle$ and cross-correlation $\langle \theta_1(t)\theta_2(0) \rangle$ functions of the orientational fluctuations. Figure 5(b) shows that the autocorrelation function decays exponentially and it can be fitted well to $\sim e^{-t/\tau_o}$ with a decay constant $\tau_o = 56$ ms. This value is comparable to the effective director relaxation time of 5CB liquid crystal ($\simeq 50$ ms) measured by the dynamic Freedericksz transition [37]. The crosscorrelation function is almost zero, suggesting that the orientational

fluctuations are not coupled hydrodynamically.

Two further comments are in order. First, the relaxation time τ of the autocorrelation function of position in the chiral NLCs is 0.64 s which is 15 times larger than that of a microsphere in water (43 ms) [21]. This is expected due to the larger flow viscosity of the liquid crystal ($\eta_{||}^{5CB} \simeq 20$ mPas) [41] with respect to that of the water ($\eta_W \simeq 1$ mPas). Secondly, although the theoretical technique adapted here is described for hydrodynamic interactions in low Reynolds number fluid systems we expect this to be valid as the Reynolds number (R_e) of NLCs is much smaller than 1 ($R_e \sim 10^{-4} - 10^{-5}$) [39, 40].

In conclusion, two collinear silica microrods aligned perpendicular to the rubbing direction in chiral nematic liquid crystals are self-trapped due to the competing effect of elastic attraction and electrostatic repulsion forming a stable bound state. The bound state is highly stable and robust against the influence of external electrical and mechanical perturbations applied by an AC electric field and the laser tweezers. In the bound state the positional fluctuations of the microrods are hydrodynamically coupled whereas their orientational fluctuations are uncoupled. The correlation relaxation time of hydrodynamic interaction in chiral nematic liquid crystals is more than one order of magnitude larger than that in aqueous suspensions. Apart from the interplay of elastic and electrostatic interactions, hydrodynamic interaction in concentrated solutions might play an important role in designing new colloidal structures with tunable properties.

Acknowledgments: SD acknowledges the support from the Department of Science and Technology, Govt. of India (DST/SJF/PSA-02/2014-2015), and DST-PURSE-II. Ravi Kumar Pujala acknowledges DST for INSPIRE Faculty Award Grant [DST/INSPIRE/04/2016/002370] and Core Research Grant [CRG/2020/006281] from SERB. P.S. acknowledges IISER Tirupati for the research funding. M.R.M acknowledges CSIR fellowship.

[1] Muševič, I. Liquid Crystal Colloids. *Springer Cham*, Switzerland **2017**.
 [2] Smalyukh, I.I. Annual Review of Condensed Matter Physics, Liquid Crystal Colloids. *Annu. Rev. Condens. Matter Phys.* **2018**, 9, 207-226.
 [3] Stark, H. Physics of colloidal dispersions in nematic liquid crystals. *Phys. Rep.* **2001**, 351 (6), 387-474.
 [4] Muševič, I.; Škarabot, M.; Tkalec, U.; Ravnik, M.; Žumer, S. Two-dimensional nematic colloidal crystals self-assembled by topological defects. *Science* **2006**, 313 (5789), 954-958.
 [5] Nych, A.; Ognysta, U.; Skarabot, M.; Ravnik, M.;

Zumer, S.; Musevic, I. Assembly and control of 3D nematic dipolar colloidal crystals. *Nat. Commun.* **2013**, 4, 1489.
 [6] Poulin, P.; Cabuil, V.; Weitz, D. A. Direct measurement of colloidal forces in an anisotropic solvent. *Phys. Rev. Lett.* **1997**, 79 (24), 4862-4865.
 [7] Tkalec, U.; Ravnik, M.; Žumer, S.; Muševič, I. Vortexlike topological defects in nematic colloids: chiral colloidal dimers and 2D crystals. *Phys. Rev. Lett.* **2009**, 103 (12), 127801.
 [8] Tkalec, U.; Ravnik, M.; Čopar, S.; Žumer, S.; Muševič, I. Reconfigurable knots and links in chiral nematic colloids.

- Science* **2011**, 333 (6038), 62-65.
- [9] Evans, J. S.; Ackerman, P. J.; Broer, D. J.; vandeLage-maat, J.; Smalyukh, I.I. Optical generation, templating, and polymerization of three-dimensional arrays of liquid-crystal defects decorated by plasmonic nanoparticles. *Phys. Rev. E* **2013**, 87 (3), 032503.
- [10] Ackerman, P. J.; Boyle, T.; Smalyukh, I. I. Squirring motion of baby skyrmions in nematic fluids. *Nat. Commun.* **2017**, 8 (1), 673.
- [11] Posnjak, G.; Čopar, S.; Mušević, I. Points, skyrmions and torons in chiral nematic droplets. *Sci. Rep.* **2016**, 6, 26361.
- [12] Jampani, V. S. R.; Škarabot, M.; Čopar, S.; Žumer, S.; Mušević, I. Chirality screening and metastable states in chiral nematic colloids. *Phys. Rev. Lett.* **2013**, 110 (17), 177801.
- [13] Jampani, V. S. R.; Skarabot, M.; Ravnik, M.; Čopar, S.; Žumer, S.; Mušević, I. Colloidal entanglement in highly twisted chiral nematic colloids: twisted loops, Hopf links, and trefoil knots. *Phys. Rev. E* **2011**, 84, 031703.
- [14] Ravnik, M.; Skarabot, M.; Žumer, S.; Tkalec, U.; Poberaj, I.; Babic, D.; Osterman, N.; Mušević, I. Entangled nematic colloidal dimers and wires. *Phys. Rev. Lett.* **2007**, 99 (24), 247801.
- [15] Munder, H.; Park, S.; Senyuk, B.; Wensink, H.H.; Smalyukh, I. I. Hybrid molecular-colloidal liquid crystals. *Science* **2018**, 360 (6390), 768-771.
- [16] Everts, J. C.; Senyuk, B.; Munder, H.; Ravnik, M.; Smalyukh, I. I. Anisotropic electrostatic screening of charged colloids in nematic solvents. *Sci. Adv.* **2021** 7 (5), eabd0662.
- [17] Munder, H.; Senyuk, B.; Smalyukh, I. I. Triclinic nematic colloidal crystals from competing elastic and electrostatic interactions. *Science* **2016**, 352 (6281), 69-73.
- [18] Stratford, K.; Gray, A.; Lintuvuori, J. S. Large Colloids in cholesteric liquid crystals. *J. Stat. Phys.* **2015**, 161 (6), 1496-1507.
- [19] Foffano, G.; Lintuvuori, J. S.; Tiribocchi, A.; Marenduzzo, D. The dynamics of colloidal intrusions in liquid crystals: a simulation perspective. *Liq. Cryst. Rev.* **2014**, 2 (1), 1-27.
- [20] Lintuvuori, J. S.; Stratford, K.; Cates, M. E.; Marenduzzo, D. Colloids in cholesterics: size-dependent defects and non-stokesian microrheology. *Phys. Rev. Lett.* **2010**, 105 (17), 178302.
- [21] Meiners, J.-C.; Quake, S. R. Direct Measurement of Hydrodynamic Cross Correlations between Two Particles in an External Potential. *Phys. Rev. Lett.* **1999**, 82 (10), 2211-2214.
- [22] Bartlett, P.; Henderson, S. I.; Mitchell, S. J. Measurement of the hydrodynamic forces between two polymer-coated spheres. *Phil. Trans. R. Soc. Lond. A* **2001**, 359 (1782), 883-895.
- [23] Skarabot, M. *et al.* Laser trapping of low refractive index colloids in a nematic liquid crystal. *Phys. Rev. E* **2006**, 73, 021705.
- [24] Mušević, I.; Škarabot, M.; Babič, D.; Osterman, N.; Poberaj, I.; Nazarenko, V.; Nych, A. Laser trapping of small colloidal particles in a nematic liquid crystal: clouds and ghosts. *Phys. Rev. Lett.* **2004**, 93 (18), 187801.
- [25] Kuijk, A.; Blaaderen, A. V.; Imhof, A. Synthesis of monodisperse, rodlike silica colloids with tunable aspect ratio. *J. Am. Chem. Soc.* **2011**, 133 (8), 2346-2349.
- [26] Rasi, M.; Pujala, R. K.; Dhara, S. Colloidal analogues of polymer chains, ribbons and 2D crystals employing orientations and interactions of nano-rods dispersed in a nematic liquid crystal. *Scientific reports* **2019**, 9, 4652.
- [27] Podolsky, D.; Banji, O.; Rudquist, P. Simple method for accurate measurements of the cholesteric pitch using a “stripe-wedge” Grandjean-Cano cell. *Liq. Cryst.* **2008**, 35 (7), 789-791.
- [28] Zuhail, K. P.; Dhara, S. Temperature dependence of equilibrium separation and lattice parameters of nematic boojum-colloids. *Appl. Phys. Lett.* **2015**, 106 (21), 211901.
- [29] Zuhail, K. P.; Dhara, S. Effect of temperature and electric field on 2D nematic colloidal crystals stabilised by vortex-like topological defects. *Soft Matter* **2016**, 12 (32), 6812-6816.
- [30] Rasi M, M.; Zuhail, K. P.; Roy, A.; Dhara, S. N-SmA-SmC phase transitions probed by a pair of elastically bound colloids. *Phys. Rev. E* **2018**, 97 (3-1), 032702.
- [31] Zuhail, K. P.; Sathyanarayana, P.; Seč, D.; Čopar, S.; Škarabot, M.; Mušević, I.; Dhara, S. Topological defect transformation and structural transition of two-dimensional colloidal crystals across the nematic to smectic-A phase transition. *Phys. Rev. E* **2015**, 91 (3), 030501(R).
- [32] Rasna, M. V.; Cmok, L.; Evans, D. R.; Mertelj, A.; Dhara, S. Phase transitions, optical, dielectric and viscoelastic properties of colloidal suspensions of BaTiO₃ nanoparticles and cyanobiphenyl liquid crystals. *Liq. Cryst.* **2015**, 42 (7), 1059-1067.
- [33] Bakker, H. E.; Hesselink, T. H.; Winjnhoven, J. E. J.; Helfferich, P. H.; van Blaaderen, A.; Imhof, A. microelectrophoresis of silica rods using confocal microscopy. *Langmuir* **2017**, 33 (4), 881-890.
- [34] Israelachvili, J. Intermolecular and surface forces (Academic Press) New York, **1992**.
- [35] Kocevar, K.; Musevic, I. Observation of an electrostatic force between charged surfaces in liquid crystals. *Phys. Rev. E* **2002**, 65, 030703(R).
- [36] Osterman, N. TweezPal – Optical tweezers analysis and calibration software. *Computer Physics Communications* **2010**, 181 (11), 1911-1916.
- [37] We measured director relaxation time $\tau_o \simeq 50$ ms using dynamic Fredericksz transition in a planar cell of 5CB at room temperature in a cell of thickness 5 μm .
- [38] Belloni, F.; Monneret, S.; Monduc, F.; Scordia, M. Multiple holographic optical tweezers parallel calibration with optical potential well characterization. *Opt. Express* **2008**, 16 (12), 9011-9020.
- [39] Lavrentovich, O. D. Active colloids in liquid crystals. *Curr. Opin. Colloid Interface Sci.* **2016**, 21, 97-109.
- [40] Sahu, D. K.; Kole, S.; Ramaswamy, S.; Dhara, S. Omnidirectional transport and navigation of Janus particles through a nematic liquid crystal film. *Phys. Rev. Res.* **2020**, 2 (3), 032009(R).
- [41] Chmielewski, A. G. viscosity coefficients of some nematic liquid crystals. *Mol. Cryst. Liq. Cryst.* **1986**, 132(3-4), 339-352.